GPS Solut (2017) 21:1469–1478
DOI 10.1007/s10291-017-0625-6

ORIGINAL ARTICLE

SBAS-derived TEC maps: a new tool to forecast the spatial maps of maximum probable scintillation index over India

Surendra Sunda[1,2] · Sneha Yadav[3] · R. Sridharan[4] · M. S. Bagiya[5] · P. V. Khekale[1] · Pan Singh[2] · S. V. Satish[2]

Received: 21 October 2016 / Accepted: 8 April 2017 / Published online: 19 April 2017

Abstract With the increase in the use of satellite-based navigation services, the forecasting of L band scintillation has turned out to be of paramount importance as it affects their accuracy and availability. Forecasting the time of occurrence or non-occurrence, strength and probable location of scintillation enables the service providers and users to take appropriate action to mitigate the effects and optimize the services. We use the recently developed method to retrieve TEC from the ionospheric correction data transmitted by the Indian satellite-based augmentation system (SBAS)–GAGAN. By making use of the established linear relation between the dusk time TEC and the maximum probable scintillation intensity (S_{4max}), scintillation forecast maps have been generated as early as 1930 LT. The superposition of actual S_4 measurements, obtained from the GAGAN network of receivers, on the forecasted S_{4max} map shows that the actual measurements are less than the predicted S_{4max} except on very few occasions. The potential of the simple technique to predict the 2 D maps of maximum probable scintillation index for the whole night has been demonstrated which with more refinements could evolve into a viable forecast or forewarning system.

Keywords Amplitude scintillation S_4 · Satellite-based augmentation system · GAGAN · TEC · EIA region

✉ Surendra Sunda
s.sunda@gmail.com

1 Space Applications Centre, ISRO, Ahmedabad, India

2 Airports Authority of India, New Delhi, India

3 Space Physics Laboratory, VSSC, Thiruvananthapuram, India

4 Physical Research Laboratory, Ahmedabad, India

5 Indian Institute of Geomagnetism, Mumbai, India

Introduction

The L band scintillations are caused by the presence of medium scale electron density irregularities, a consequence of a hierarchy of plasma instabilities initiated primarily by the Rayleigh–Taylor instability during post-sunset hours and generally referred as equatorial spread F (ESF). One of the severest manifestations of the instability process is the generation of the plasma bubbles, which are depleted plasma density regions that are initiated at the bottom of the F-layer over the magnetic equator and evolve nonlinearly through the topside ionosphere. Due to their field-aligned nature, these irregularities map down along the magnetic field lines toward higher latitude F-region, the extent of which would depend upon the altitudinal extent over the magnetic equator. It often extends to the crest latitudes of the equatorial ionization anomaly (EIA: about ±15° of the magnetic equator). By virtue of the large background ionization density at the crest locations and the consequent steeper gradients becoming available for the plasma instability, the situation becomes conducive for strong irregularities and consequent intense scintillations. Trans-ionospheric radio waves propagating through the region of density irregularities undergo severe fading and fluctuations in amplitude (S_4 index) and phase (σ_φ index) due to diffraction and refraction. The strong scintillation may lead to loss of lock of the satellite signal, thereby affecting the accuracy and availability of the satellite-based navigation services (Sunda et al. 2013). It could be appreciated that with the advent of GPS and other global and regional satellite navigation systems (GLONASS, Galileo, BeiDou, IRNSS and QZSS), the satellite-based navigation has emerged as the primary navigational aid even in life critical applications like aircraft navigation. Hence, understanding the basic physical processes, which control and modulate the occurrence pattern of scintillations with a goal to be able to forecast, is considered of paramount importance and has remained a formidable task till recently.

As the occurrence of scintillation is a natural phenomenon of very large proportions, the question of mitigating the scintillations themselves does not arise. The other alternatives being to design the ground receiver such that it would not lose its synchronization even in extreme scintillation events or be ready with accurate forecasts of both the spatial and temporal occurrence pattern of the scintillations to avoid the regions infested with irregularities at any specific instant. The former is a technological challenge and demands very fast reacquisition capability of the receiver (Seo et al. 2009), while the other option of the accurate forecast is turning out to be more practical to circumvent the problem. In recent times, several studies highlighting the role of post-sunset equatorial electrodynamics (Anderson et al. 2004; Tulasiram et al. 2006), and the control of EIA (Thampi et al. 2006; Manju et al. 2011) on the occurrence pattern of scintillations have been carried out. On the other hand, de Lima et al. (2015) attempted to forecast the scintillations using neural networks. The morphology of L band scintillations has also been studied extensively in recent years. Now it is well established that scintillation occurs after sunset and typically extends up to 2 h after midnight (Rama Rao et al. 2006) having the maximum probability between 2000 and 2230 local time (Sunda et al. 2014). The equinoctial months (March/April and September/October) are more favorable for the scintillation activity over Indian longitudes. Over all, the time, intensity and occurrence rate of scintillation depends on the probing frequency, solar cycle, geomagnetic activity, location, and season (Aarons 1982; Tsunoda 1985; Groves et al. 1997). However, the most enigmatic aspect is the day-to-day variability of scintillation (Tsunoda 2005).

Significant work has been done in the past in identifying the favorable background ionospheric and thermospheric conditions that make it conducive for the plasma instabilities to operate. After local sunset, in the absence of production of ionization, the bottom side F-region decays while the equatorial F-layer moves upward due to the prereversal enhancement (PRE) of the eastward zonal electric field. This uplifting of the F-layer base creates an analogous situation of a heavier fluid being supported by a lighter fluid. Under such unstable conditions, electron density perturbations if any, at the base of the F-region could initiate the Rayleigh–Taylor instability which would, in turn, allow the perturbations to grow in amplitude and extend in altitude. In the past, attempts had been made to forecast the day-to-day occurrence of scintillation based on the background ionospheric and thermospheric conditions without paying much attention to the variability during a single night (Anderson et al. 2004; Redmon et al. 2010). However, in recent times, the possible role of the seed perturbations like gravity waves (Abdu et al. 2009; Sreeja et al. 2009) and also large-scale wave structures (LSWS) (Saito and Maruyama 2007; Tsunoda et al. 2011) in controlling its variability have been addressed. Further, Bagiya and Sridharan (2011) brought out the close relation between the characteristic features of the perturbations and also the different manifestations of ESF like plumes in the VHF radar and the L band scintillation. They concluded that, by getting a handle on the characteristics of perturbation in the F-region well before the actual occurrence of the irregularities, with the other background conditions permitting, the evolutionary pattern of the same during the night could be forecast.

It could well be appreciated that the requirements for operational level forecasts are with the sole aim of keeping the potential user prepared, rather over-prepared to the impending ionospheric conditions. For example, the fundamental questions such as the likelihood of occurrence or non-occurrence of scintillation on a particular day, and if in affirmative, then other parameters need to be addressed such as 'when (LT),' 'where (longitude zones),' maximum 'duration,' and the maximum 'strength' in addition to the 'latitudinal extent' of the scintillation region. The operational forecast should provide the worst-case situation so as to safeguard the interests of the potential user. In this direction, Sridharan et al. (2012) evolved a method based on GPS total electron content (TEC) to forecast 'when' and for 'how long' the scintillation patches are likely to occur over a location. Bagiya et al. (2014) further refined the method by considering the fluctuations in the critical frequency of the F-region $[f_0F_2]^2$ over the dip equator as truly representing the perturbations in the F-region instead of the TEC fluctuations. After making a reasonable forecast for the temporal evolution of L band scintillation over Trivandrum (8.5°N, 76.91°E; dip latitude 0.5°N), Sridharan et al. (2014) succeeded in generating the spatiotemporal forecast map of the occurrence pattern over the Indian region with a basic knowledge of the zonal velocity of the perturbations. It was further fine tuned by Bagiya et al. (2015) by taking into account the zonal velocity variations determined by using the scintillation data from two geostationary satellites (GSAT-8 and GSAT-10).

Though the results from the above studies provided the spatiotemporal occurrence patterns, one of the important aspects, i.e., the probable maximum strength of the scintillation had not been provided as a forecast parameter. In other words, very strong and weak scintillation has not been differentiated in the earlier studies, which is crucial for satellite-based navigation applications. We address this least explored aspect.

Approach

Scintillation index, S_4, which is essentially a normalized standard deviation of the signal intensity over 60 s, is a widely used parameter to define the strength of amplitude scintillation. The total S_{4T}, including the effects of ambient noise, is defined as follows (Van Dierendonck and Quyen 2001):

$$S_{4T} = \sqrt{\frac{\langle SI^2 \rangle - \langle SI \rangle^2}{\langle SI \rangle^2}} \quad (1)$$

where $\langle\rangle$ represents the expected (or average) value over the interval of interest (typically 60 s).

In order to measure the S_4 index precisely, scintillation monitoring receivers require high sampling rates (typically 50 Hz) and use stable clocks (OCXO). The Airports Authority of India (AAI) and the Indian Space Research Organization (ISRO) have set up a network of scintillation monitoring receivers under the Indian SBAS project–GAGAN (GPS Aided GEO Augmented Navigation) in the year 2004. As a part of this project, 23 GSV4004A/B receivers (housing Novatel's Euro4/OEM4G2 cards) are operational, which provide the measurements of total S_4 (S_{4T}) and S_4 correction due to ambient noise (S_{4C}) at a 1-min interval along with TEC. Figure 1 shows the location of the TEC and scintillation monitoring receivers in India under GAGAN project. The true and corrected value of S_4 is calculated using the formula:

$$S_4 = \sqrt{S_{4T}^2 - S_{4C}^2} \quad (2)$$

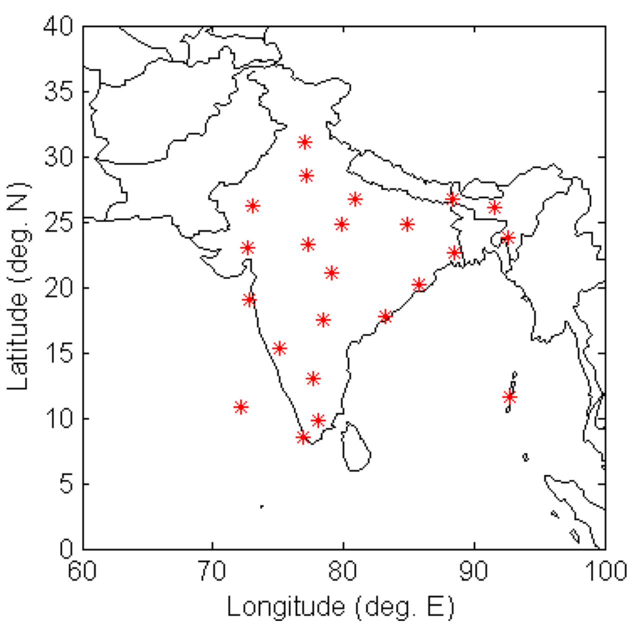

Fig. 1 TEC and scintillation monitoring receivers (GSV4004) operating under the GAGAN project over Indian region

In case S_{4C} turns out to be higher than S_{4T}, then S_4 is set to zero (Van Dierendonck and Quyen 2001). The ideal range of S_4 is 0–1, but sometimes it may even be up to 1.2.

It is well established that the strength of scintillation shows a good correlation with the background electron density distribution in the local ionosphere (Basu et al. 1988; Whalen 2009; Chakraborty et al. 2012). The vertical TEC is one of the more easily available parameters to represent the background electron density distribution over any location. Further, the post-sunset enhancement in the zonal electric field, caused by activation of the F-region dynamo after local sunset, rejuvenates the equatorial ionization anomaly (EIA) resulting in the maximum plasma density at any given location over the entire EIA region. In the absence of fresh production of ionization and also in the absence of transport from other regions, the ion concentration over any location is bound to decrease with time due to recombination. In other words, after sunset and extending into the night time, the post-sunset TEC over any location is expected to be the maximum for the whole of the night.

Making use of the evening time TEC_{1930} and S_4 index obtained from one of the GAGAN-TEC network stations. Trivandrum (8.5°N, 76.5°E, 0.5°N dip lat), during 2005–2011 and using about 105 scintillation events in equinoctial months, Bagiya et al. (2013) derived the best fit linear relationship as:

$$S_{4\max} = 0.01302 \times TEC_{1930} + 0.04795 \quad (3)$$

where $S_{4\max}$ is the maximum probable strength of scintillation and TEC_{1930} is the averaged vertical TEC (VTEC) between 1830 and 1930 h local time. It had been shown that on all the occasions considered, the actual S_4 had been less than what has been forecasted based on the linear relation, implying that operational forecasts of S_4 could be based on the a priori knowledge of TEC_{1930} over any location. This will prepare the potential user for the possible worst-case situation. The above simple approach should be viewed in the light of the discussion by de Lima et al. (2015) wherein they had attempted to predict the strength of scintillation over the magnetic equator using neural network techniques and had highlighted (i) the complexities involved and (ii) the limitations of such techniques. This linear relationship is in line with earlier works on maximum electron density, $N_{\max}$ and S_4 (Dabas et al. 1988; Whalen 2009). Since vertical TEC is mostly governed by $N_{\max}$ which dominates the total electron content, we have taken TEC_{1930}, which could be directly obtained from the GPS satellites, to represent the evening time background densities. It implies that if we have prior knowledge on the TEC distribution at 1930 LT over any region, we should in principle be able to generate the $S_{4\mathbf{max}}$

maps as early as 1930 LT that would represent the region under consideration for the entire night. However, this requirement would call for real-time access of the TEC from a very large area dominated by equatorial electrodynamical processes like the highly variable EIA and the consequent variation in the spatiotemporal plasma density distribution. Conventional dual-frequency GPS receiver data, even if available for the entire region, may be useful for post-facto analysis but are not suited for operational forecasting applications due to the constraints in pooling the data and also due to the need to account for factors like the satellite and receiver biases before generating a TEC map. In the present study, an innovative utilization of satellite-based augmentation system (SBAS) technique proposed by Sunda et al. (2015) will be used to obtain TEC_{1930}, and for forecasting the maximum probable strength of scintillation index (S_{4max}). Comparison of the forecast maps with actual occurrence of scintillations reveals the potential of the suggested technique in providing a basic operational tool for satellite-based navigation. The details are provided below.

TEC determination from SBAS

The primary requirement of vertical TEC for operational forecasting over a wide region can be met by the technique proposed by Sunda et al. (2015) to derive the vertical TEC from grid-based ionospheric corrections broadcast by the SBAS geostationary satellite. Currently, there are four operational SBAS systems worldwide—WAAS (US), EGNOS (Europe), MSAS (Japan) and GAGAN (India). The typical configuration of any SBAS would consist of a network of Reference Stations, a Master Control Center (MCC) and an Uplink Station along with the geostationary SBAS satellites. Figure 2 shows the configuration of Indian SBAS–GAGAN which consists of 15 Reference Stations (INRES), three Master Control Centers (INMCC), and three Uplink Stations (INLUS). There are three geostationary satellites—GSAT-8 at 55°E (PRN 127), GSAT-10 at 82°E (PRN 128) and GSAT-15 at 83°E(PRN -132, spare) in orbit for GAGAN broadcast. The Reference Stations would collect and preprocess the dual-frequency measurements from visible GPS/GNSS satellites and send the data to MCC at every second. The MCC processes the data collected from all Reference Stations to derive the ephemeris, clock and ionospheric errors. Finally, these error corrections along with integrity information are converted into 250 bit navigation messages known as Message Types (MT). The MTs are numbered from 0 to 63, and most of them are reserved for future use. These navigation messages are uplinked to the geostationary SBAS satellite in C band. The bend pipe transponder on the SBAS satellite down converts these messages to L1 frequency and broadcast back to the ground. The PRN codes of SBAS satellites are similar to GPS and have been assigned numbers in the range of 120–158. This will ensure that single-frequency (L1) GPS user receiver will acquire the SBAS signal for necessary corrections in positioning.

It is to be noted that the ephemeris and clock errors are scalar quantities specific to a satellite whereas the ionospheric errors are spatial in nature and need vector corrections. Hence, the globe is divided into vertical and horizontal bands to define the Ionospheric Grid Points (IGPs). The pre-defined IGPs are separated by 5° × 5° latitude and longitude over low and mid-latitudes and by 10° × 10° at higher latitudes. The SBAS system broadcasts the ionospheric corrections in the form of Grid Ionospheric Vertical Delay (GIVD) in meters for L1 frequency along with its variance known as Grid Ionospheric Vertical Error (GIVE) at pre-specified IGPs in Message Type 26 (MT26). Another message MT18 provides the information regarding the IGPs served by the particular SBAS, which needs to be decoded before the application of ionospheric corrections. The Indian SBAS–GAGAN broadcasts the GIVD for 102 IGPs over the Indian subcontinent (5°S to 45°N and 55°E to 110°E), which gets updated about every 5 min and hence provide near real-time information about the service area. It is worthy to mention here that the ionospheric delay at any frequency is proportional to the TEC. The vertical delay of 1 m at L1 corresponds to about 6 TEC Units (1 TECU = 10^{16} e/m^2). Data from any GPS receiver with an inbuilt SBAS channel can be decoded to derive the vertical delay (equivalent to TEC) corresponding to the IGPs served by the particular SBAS. Moreover, being in equatorial and low latitude region, GAGAN, in particular, has found its usefulness in generating the real-time TEC maps depicting the dynamical spatiotemporal features of EIA (Yadav et al. 2016).

Keeping in mind the potential advantage of SBAS in providing online TEC information, the averaged VTEC during 1830–1930 LT (TEC_{1930}) is determined at each grid point. It also makes sense utilizing the SBAS since the whole scheme is aimed at satellite-based navigation users. Thus, it would be easier to integrate and implement the proposed forecasting methodology as a part of the navigation scheme in future. The averaged VTEC values for the entire Indian region can now be used to estimate the scintillation intensity using the linear relation shown in (3). However, in light of usable forecast maps, it becomes essential to indicate the maximum latitude region that is likely to get affected due to the presence of the ionospheric irregularities. Bagiya et al. (2013) had shown that the base height of the F-region *h’F* at 1930 local time bears a relation to the maximum altitudinal spread of the irregularities during the night, which due to its field-aligned nature would extend in latitude along the magnetic field

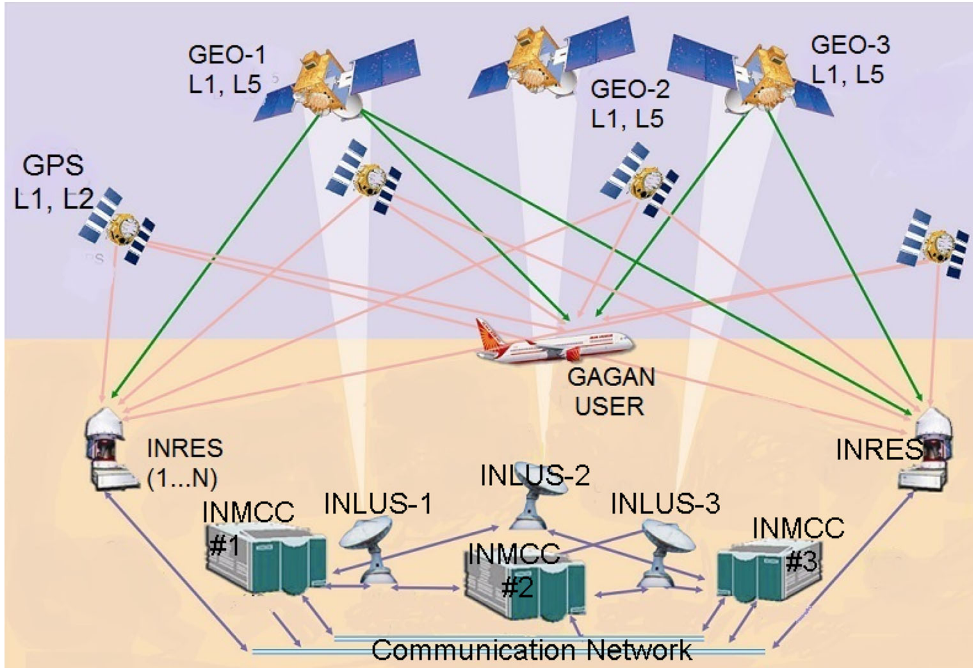

Fig. 2 Configuration of Indian SBAS–GAGAN (Courtesy AAI/ISRO). It consists of 15 Reference Stations (INRES), three Master Control Centers (INMCC) and three Uplink Stations (INLUS). The space segment consists of three geostationary satellites—GSAT-8 at 55° E (PRN 127), GSAT-10 at 82° E (PRN 128) and GSAT-15 at 83° E (PRN 132, spare) for broadcasting the GAGAN navigation messages

lines. Making use of this information, the upper latitude limits have been estimated for the days under consideration beyond which it has been shown as a scintillation-free region (by dashed rectangular boxes) in the S_4 maps.

Finally, in order to verify and validate the proposed method, the estimated maximum value of $S_{4\mathbf{max}}$ during a given night is compared with the actual measurement of S_4 taken from the scintillation monitoring receivers operating under the GAGAN-TEC network. The results are presented and discussed below.

Results and discussion

Before discussing the results, it is reiterated that this research deals with forecasting the maximum strength of scintillation, i.e., $S_{4\max}$ over a given night with an emphasis on the day-to-day variation. With this in mind, we selected three different days in April 2012 during which a campaign was carried out from the equatorial station Trivandrum in India.

Figure 3 is a TEC map of averaged VTEC during 1830-1930 LT (TEC_{1930}) on April 26, 2012 derived from the GAGAN broadcast of ionospheric delay corrections at the specified grid points over the Indian subcontinent. The color-coded circles at the IGPs (5° lat × 5° long) represent the TEC_{1930} at that point. The linear interpolation technique is used to create the contour plots. The significant large-scale features like the EIA are clearly discernible in the figure with a steep latitudinal gradient in TEC till the

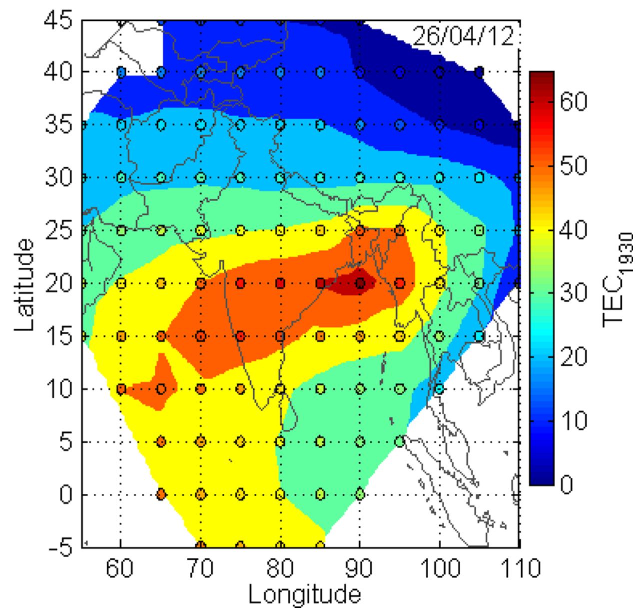

Fig. 3 Evening time TEC contour map of averaged VTEC during 1830–1930 local time on April 26, 2012 over the Indian subcontinent. The circles are the pre-defined ionospheric grid points (102 IGPs) where GAGAN broadcasts the ionospheric delay information, and their linear interpolation has resulted in the contour plot. The *color* in each *circle* denotes the averaged vertical TEC (TEC_{1930})

location of the crest of EIA around 20°N latitude (geographic), beyond which it steadily decreased.

With the availability of TEC_{1930} for the entire region, it becomes straightforward to translate it into maximum probable $S_{4\mathbf{max}}$ by using the linear Eq. (3). Figure 4 illustrates the $S_{4\mathbf{max}}$ likely to occur over the Indian subcontinent

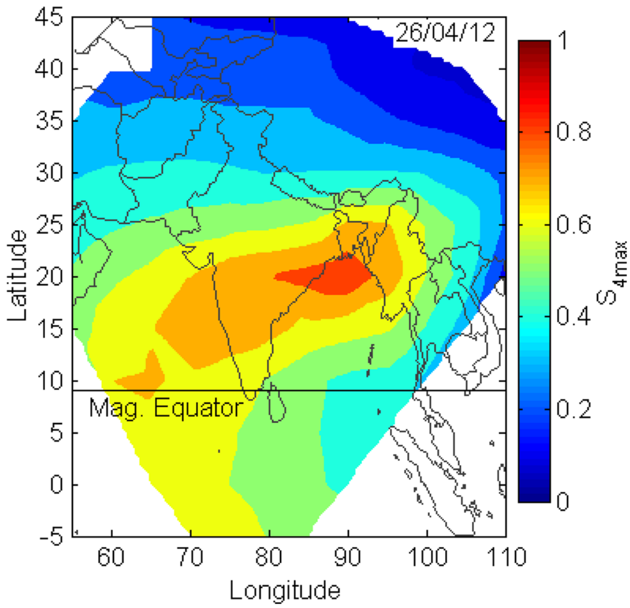

Fig. 4 Forecasted strength of scintillation S_{4max} on April 26, 2012. S_{4max} is mapped from the VTEC shown in Fig. 3 using the linear relationship with TEC_{1930} as per Eq. (3). The *horizontal line* depicts the magnetic equator passing through southern part of India

during that night. In other words, if and when scintillations occur over any particular location, the projected $\mathbf{S_{4max}}$ would be the maximum for the entire night. From the forecasting point of view, if the actual S_4 happens to be less than the maximum projected value, it would still be acceptable since the forecast had only kept the user prepared for a probable worst-case situation. Though the scintillation would be constrained to be within the set limits indicated above, its actual occurrence pattern would be decided by the background ionospheric–thermospheric conditions and also the nature of the perturbations. In the earlier studies, though the spatiotemporal maps were successfully generated (Bagiya et al. 2014; Sridharan et al. 2014), the intensity aspect of the scintillations was not addressed. The present work enables one to deal with this point through the generation of TEC maps and by making use of the relation between the TEC_{1930} and $\mathbf{S_{4max}}$. We restrict ourselves here to compare the actual occurrence pattern of scintillations during the entire night and demonstrate the efficacy of the proposed scheme.

The data from the GAGAN-TEC network that consists of 23 TEC and scintillation monitoring receivers are used for S_4 measurements over the Indian region. Since the low elevation satellites are prone to multi-path-induced scintillations, an elevation mask angle of 40° is considered for selecting the S_4 measurements. Following Spogli et al. (2009), these measurements are projected to the vertical by accounting for the geometrical effects at different elevation angles. The measured S_4 values for April 26, 2012, represented by colored circles corresponding to the respective ionospheric pierce points (IPPs) of the GAGAN-TEC network stations, are superimposed on the forecasted strength of $\mathbf{S_{4max}}$ in Fig. 5. It may be noted that the size of the circle and its color is a measure of the strength of measured S_4 index. All the S_4 measurements greater than 0.3 ($S_4 > 0.3$) from all satellites and all stations are taken into account to display at their respective IPPs. Based on the *h'F* values at 1930 h, the latitudinal extent of scintillation predicted (Bagiya et al. 2013) for this day turns out to be 18.86°N magnetic latitude (27.86°N geographic latitude) beyond which the region is expected to be scintillation free, and this has been depicted in the figure by a dashed rectangular box. True to the expectation of the forecast scheme, latitudes beyond 27.86°N remained scintillation free. Focusing on the scintillation-prone region, it can be noted that almost all the measured S_4 values are lower than the forecasted S_{4max} with very few exceptions. Though the results of the comparison are encouraging, the few exceptions still need to be studied in greater detail with a larger data set and an in-depth analysis of TEC and S_4 relationship. The reliability of the results in the light of the deviations is discussed later.

The notable result is the consistently lesser value of S_4 than the forecasted $\mathbf{S_{4max}}$ vindicating the established relation between TEC_{1930} and the $\mathbf{S_{4max}}$ and the overall

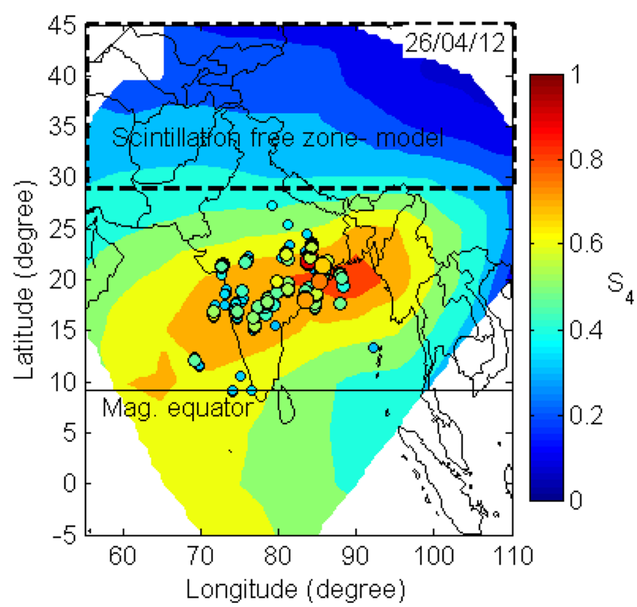

Fig. 5 Comparison of forecasted scintillation strength with actual measurements of the S_4 index on April 26, 2012, a moderate EIA day. The *circles* denote the S_4 measurements at different ionospheric pierce points (IPPs) observed by ground stations. The *color code* inside *circles* depicts the strength of measured scintillation—S_4 index. The *dashed rectangular* region represents the scintillation-free zone above the latitudinal extent of scintillation as inferred from the *h'F* at 1930 h LT over the magnetic equator (Bagiya et al. 2013)

occurrence pattern of actual scintillation that closely follows the forecast including the replication of the tongue-like structure of TEC_{1930}. Another spectacular example of intense scintillations could be seen in Fig. 6 for April 28, 2012. One could notice the well-developed EIA and the orientation of the scintillation occurrence pattern bearing semblance to the forecasted S_{4max} and at the same time consistently remaining lower. Furthermore, a typical example corresponding to a weak to moderate scintillation day (April 21, 2012) is shown in Fig. 7. On this day, the EIA had been rather weak and so is the S_4 intensity pattern. Nevertheless, the orientation of observed S_4 pattern along with that of the forecasted S_{4max} stands out.

On all the three occasions, it could be seen that the forecasted scintillation-free region remained, thus confirming the validity of the approach. In order to add more credence to the forecast scheme and to put the results on a quantitative footing, the maximum observed scintillation in each 2 × 2 degree (lat/long) bin is compared with the predicted scintillation corresponding to that bin. Figure 8 shows the predicted S_{4max} with the observed S_{4max} for all the 3 days combined. The prediction line is drawn to illustrate the deviation which is about 2% during the period under study.

The exceptions, though very small, could be due to two reasons. First, the inherent inaccuracy in SBAS TEC values, and secondly, the scatter in the TEC_{1930} versus S_4 plots (Bagiya et al. 2013) and the deviation of the best fit curve used for the generation of the S_{4max} maps. To probe

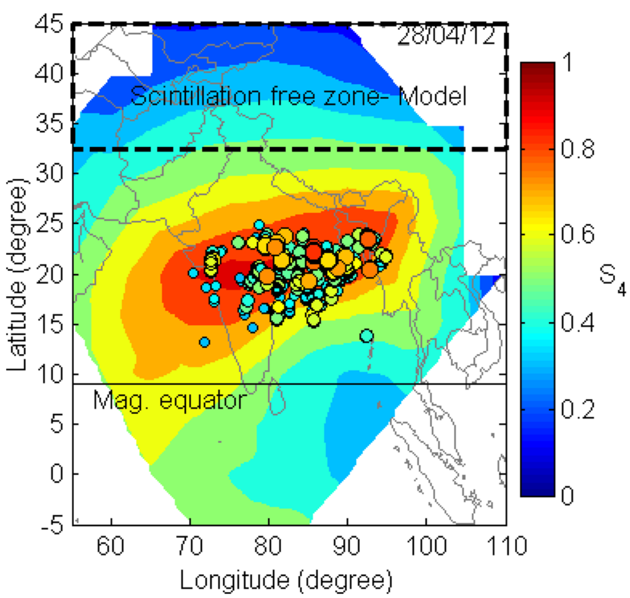

Fig. 6 Example depicting the forecast of intense scintillations (Strong S_{4max}) as a consequence of the presence of strong EIA at 1930 LT and actual S_4 observations for April 28, 2012. A clear cut orientation of the spatial occurrence of scintillations as per the forecast could be seen

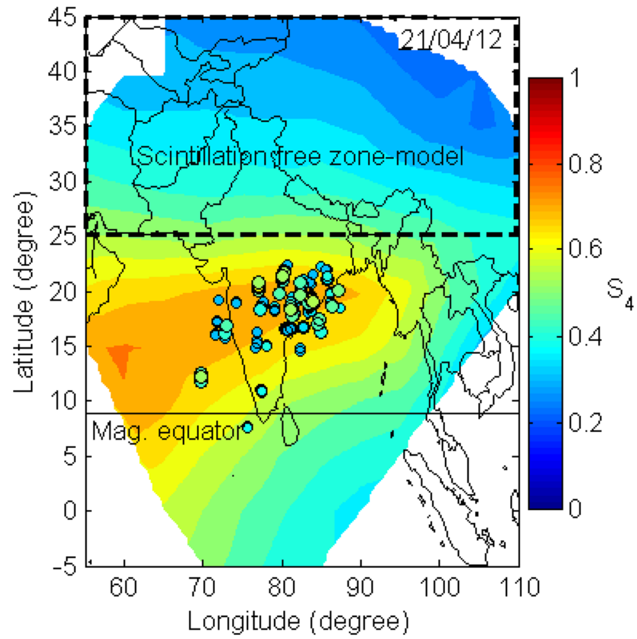

Fig. 7 Representative example on a weak EIA and consequent weaker scintillations on April 21, 2012. Though sparse, the occurrence pattern still follows the forecast and is consistently lower than the forecast S_{4max}

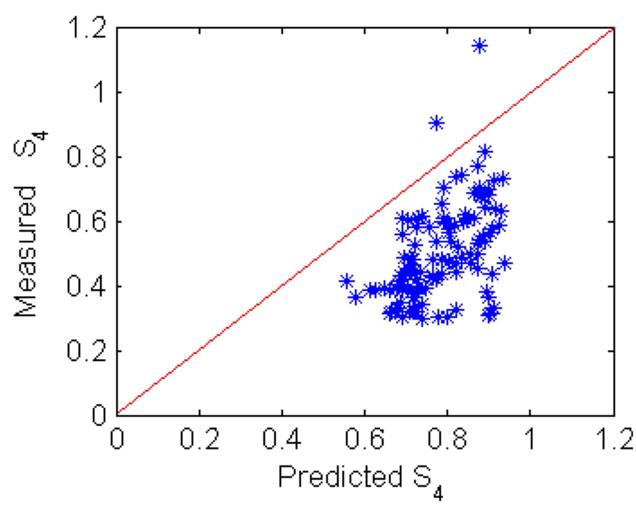

Fig. 8 Quantitative comparison of predicted S_{4max} with the observed S_{4max} for all the 3 days put together. The maximum observed scintillation in each 2 × 2 degree bin is compared with the corresponding predicted scintillation. The observed S_{4max} turned out to be more than forecasted only on about 2% of the occasions

the first aspect, the SBAS-generated TEC is compared with the GPS measured TEC, considered as 'true' TEC (referred as Truth). For this, a representative ground station, Bhubaneshwar (20.25°N, 85.8°E), which is located close to an IGP (20°N, 85°E) and essentially lying in the crest region of EIA is selected. The comparison as shown in Fig. 9 clearly brings out the good agreement between SBAS TEC and Truth on all the selected days used. The

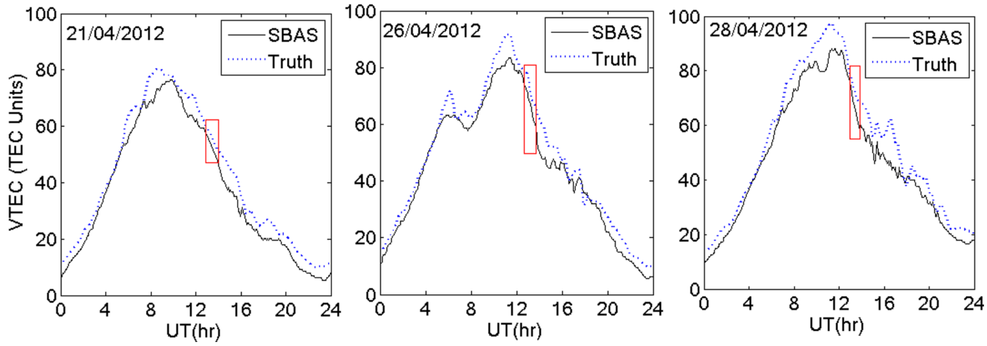

Fig. 9 Comparison of SBAS-generated TEC (*solid line*) with GPS (Truth) measurements (*dash line*) at one of the ground station of the GAGAN-TEC network, Bhubaneshwar (20.25°N, 85.8°E) lying close to IGP (20, 85), for three days used in this study. The difference of averaged TEC during the interested time period indicated by the rectangular box is 3.7, 7.4 and 7 TEC on April 21, 26 and 28, 2012, respectively

difference of averaged TEC during 1830–1930 LT, as indicated by the rectangular box in the figure, is found to be 3.7 TEC, 7.4 TEC and 7 TEC units on April 21, 26, and 28, 2012, respectively. This difference is negligible in terms of predicted S_{4max} using (3). However, more statistics is needed to ascertain the accuracy of SBAS TEC values. Furthermore, the SBAS broadcast error bound, GIVE, can be potentially utilized to provide the variance of the predicted S_{4max}. It is believed that model Eq. (3) can be improved with a larger database to reduce the discrepancies, if any, in the forecast.

In the above exercises, the forecasts only show the $S_{4\mathbf{max}}$ maps, corresponding to the TEC_{1930}. The scintillations maps presented thus far are not intended to show the instantaneous spatial occurrence pattern in the region of interest and its temporal variation. To accomplish such a dynamical map, a moving pattern of the perturbation wave train (considering only the negative phase of the perturbation) has to be superposed over the forecast map to arrive at the spatial map at every instant. In other words, a moving template of the negative phase of the perturbation over the S_{4max} map would show the regions of scintillation and/or no-scintillation at every instant. This will enable a dynamical forecast to a reality and will enable the user, like an aircraft to take corrective measures at critical times and locations. Such an exercise is beyond the scope of the present study. As the first step in this direction, we arrive at the S_{4max} corresponding to every location for the entire night. This amounts to stating that, if scintillations occur at any location, the observed S_4 would be less than the forecasted $S_{4\mathbf{max}}$. The case study carried out for three different days representing different geophysical conditions and scintillation intensities amply demonstrates the potential of the present method. The next logical step would be to evolve a dynamical map that would highlight the regions of irregularity in near real time.

Summary

Satellite-based navigation is gaining importance in life critical applications like civil aviation. However, it is vulnerable to the ionospheric scintillations which can cause loss of lock of the satellite signal, thus affecting the accuracy and availability of vital position information. Therefore, forecasting the occurrence pattern of the ionospheric scintillation along with its maximum probable intensity has become extremely important. Once indicative forecasts have become available, it would serve as a warning to the user so as to be prepared well in time to take counter measures. An established relation between the dusk time vertical TEC (TEC_{1930}) and the maximum probable S_{4max} is used to predict the maximum intensity of scintillation on a given night. The spatiotemporal vertical TEC is retrieved by employing the innovative method of utilizing the ionospheric corrections broadcast by SBAS at pre-defined ionospheric grid points (IGPs). The simplicity of fetching the SBAS data in real time makes it possible to generate the S_{4max} maps that would be valid for the whole night. The spatial pattern of the actual scintillations is well aligned with the S_{4max} distribution. The actual scintillation intensity turns out to be less than what has been forecasted for S_{4max}. The current study presents an integrated picture and demonstrates that a viable forecast map indicating not only the spatial occurrence pattern but also the intensity of maximum probable scintillations would soon become a reality.

Acknowledgements The data used in the study are part of the GAGAN project, a joint collaboration between AAI and ISRO. S.S. duly acknowledges the AAI for the support and SAC (ISRO) for hosting his position. R.S. duly recognize the National Academy of Sciences Allahabad for the NASI Sr. Scientist position and also director PRL for hosting the positions.

References

Aarons J (1982) Global morphology of ionospheric scintillations. Proc IEEE 70(4):360–378

Abdu MA, Alam Kherani E, Batista IS, de Paula ER, Fritts DC, Sobral JHA (2009) Gravity wave initiation of equatorial spread F/plasma bubble irregularities based on observational data from the spread F-Ex campaign. Ann Geo- phys 27(7):2607–2622

Anderson DN, Reinisch B, Valladare C, Chau J, Veliz O (2004) Forecasting the occurrence of ionospheric scintillation activity in the equatorial ionosphere on a day-to-day basis. J Atmos Terr Phys 66(17):1567–1572

Bagiya MS, Sridharan R (2011) Evolutionary phases of equatorial spread F including L band scintillations and plumes in the context of GPS total electron content variability: a case study. J Geophys Res 116:A10304. doi:10.1029/2011JA016893

Bagiya MS, Sridharan R, Sunda S (2013) Pre-assessment of the "strength" and "latitudinal extent" of L band scintillation: a case study. J Geophys Res Space Phys 118(1):488–495. doi:10.1029/2012JA017989

Bagiya MS, Sridharan R, Sunda S, Jose L, Pant TK, Choudhary R (2014) Critical assessment of the forecasting capability of L band scintillation over the magnetic equatorial region—campaign results. J Atmos Sol Terr Phys 110–111:15–22

Bagiya MS, Sridharan R, Sunda S, Jose L, Pant TK, Choudhary R (2015) Impact of the perturbation zonal velocity variation on the spatio/temporal occurrence pattern of L band scintillation —A case study. J Geophys Res Space Phys 120(7):5882–5889. doi:10.1002/2015JA021322

Basu S, MacKenzie E, Basu Su (1988) Ionospheric constraints on VHF/UHF communication links during solar maximum and minimum periods. Radio Sci 23(3):363–378

Chakraborty SK, Hajra R, DasGupta A (2012) Ionospheric scintillation near the anomaly crest in relation to the variability of ambient ionization. Radio Sci 47(2):RS2006. doi:10.1029/2011RS004942

Dabas RS, Lakshmi DR, Reddy BM (1988) Day-to-day variability in the occurrence of equatorial and low-latitude scintillations in the Indian zone. Radio Sci 33(1):89–96

de Lima GRT, Stephany S, de Paula ER, Batista IS, Abdu MA (2015) Prediction of the level of ionospheric scintillation at equatorial latitudes in Brazil using a neural network. Space Weather 13(8):446–457. doi:10.1002/2015SW001182

Groves KM et al (1997) Equatorial scintillation and systems support. Radio Sci 32(5):2047–2064. doi:10.1029/97RS00836

Manju G, Sreeja V, Sudha Ravindran S, Thampi SV (2011) Toward prediction of L band scintillation in the equatorial ionization anomaly region. J Geophys Res 116:A02307. doi:10.1029/2010JA015893

Rama Rao PVS, Gopikrishna S, Niranjan K, Prasad DSVVD (2006) Study of spatial and temporal characteristics of L-band scintillations over the Indian low latitude region and their possible effects on GPS navigation. Ann Geophys 24(6):1567–1580

Redmon RJ, Anderson D, Caton R, Bullett T (2010) A forecasting ionospheric real-time scintillation tool (FIRST). Space Weather 8(12):S12003

Saito S, Maruyama T (2007) Large-scale longitudinal variation in ionospheric height and equatorial spread-F occurrences observed by ionosondes. Geophys Res Lett 34(16):L16109. doi:10.1029/2007GL030618

Seo J, Walter T, Chiou TY, Enge P (2009) Characteristics of deep GPS signal fading due to ionospheric scintillation for aviation receiver design. Radio Sci 44(1):RS0A16

Spogli L, Alfonsi L, De Franceschi G, Romano V, Aquino MHO, Dodson A (2009) Climatology of GPS ionospheric scintillations over high and mid-latitude European regions. Ann Geophys 27(9):3429–3437. doi:10.5194/angeo-27-3429-2009

Sreeja V, Vineeth C, Pant TK, Ravindran S, Sridharan R (2009) Role of gravity wavelike seed perturbations on the triggering of ESF—A case study from unique dayglow observations. Ann Geophys 27(1):313–318

Sridharan R, Bagiya MS, Sunda S (2012) A novel method based on GPS TEC to forecast L band scintillations over the equatorial region through a case study. J Atmos Sol Terr Phys 80:230–238

Sridharan R, Bagiya MS, Sunda S, Choudhary R, Pant TK, Jose L (2014) First results on forecasting the spatial occurrence pattern of L band scintillation and its temporal evolution. J Atmos Sol Terr Phys 119:53–62

Sunda S, Vyas BM, Satish SV, Khekale PV, Parikh KS (2013) Improvement of position accuracy with GAGAN and the impact of scintillation on GNSS. Positioning 4:282–288. doi:10.4236/pos.2013.44028

Sunda S, Vyas BM, Khekale PV, Parikh KS, Satish SV, Sudhir CR, Ganeshan AS, Gera V (2014) Statistically characterizing the L-band scintillation over Indian equatorial and low latitude region. In: Proceedings of general assembly and scientific symposium (URSI GASS), 2014 XXXIth URSI, Beijing, pp 1–4. doi:10.1109/URSIGASS.2014.6929754

Sunda S, Sridharan R, Vyas BM, Khekale PV, Parikh KS, Ganeshan AS, Sudhir CR, Satish SV, Bagiya MS (2015) Satellite-based augmentation systems: a novel and cost-effective tool for ionospheric and space weather studies. Space Weather 13(1):6–15. doi:10.1002/2014SW001103

Thampi SV, Ravindran S, Pant TK, Devasia CV, Sreelatha P, Sridharan R (2006) Deterministic prediction of post-sunset ESF based on the strength and asymmetry of EIA from ground based TEC measurements: preliminary results. Geophys Res Lett 33(13):L13103. doi:10.1029/2006GL026376

Tsunoda RT (1985) Control of the seasonal and longitudinal occurrence of equatorial scintillations by the longitudinal gradient in integrated E region Pedersen conductivity. J Geophys Res 90(A1):447–456. doi:10.1029/JA090iA01p00447

Tsunoda RT (2005) On the enigma of day to day variability in equatorial spread-F. Geophys Res Lett 32(8):L08103. doi:10.1029/2005GL022512

Tsunoda RT, Yamamoto M, Tsugawa T, Hoang TL, Tulasi Ram S, Thampi SV, Chau HD, Nagatsuma T (2011) On seeding, large-scale wave structure, equatorial spread F, and scintillation over Vietnam. Geophys Res Lett 38(20):L20102. doi:10.1029/2011GL049173

Tulasiram S, Rama Rao PVS, Niranjan K, Prasad DSVVD, Sridharan R, Devsia CV, Ravindran S (2006) The role of post-sunset vertical drifts at the equator in predicting the onset of VHF scintillations during high and low sunspot activity years. Ann Geohpys 24:1609–1616

Van Dierendonck AJ, Hua Quyen (2001) Measuring Ionospheric Scintillation Effects from GPS Signals. Proc. ION AM 2001, Institute of Navigation, Albuquerque, NM, USA, June 11-13, 391-396

Whalen JA (2009) The linear dependence of GHz scintillation on electron density observed in the equatorial anomaly. Ann Geophys 27(4):1755–1761

Yadav S, Sunda S, Sridharan R (2016) The impact of the 17 March 2015, St Patrick's day storm on the evolutionary pattern of equatorial ionization anomaly over the Indian longitudes using high resolution spatio temporal TEC maps: new insights. Space Weather 14(10):786–801. doi:10.1002/2016SW001408

Surendra Sunda received B.E. (Electronics and Communication) from Govt. Engineering College, Kota in 2000 and M.Tech (Communication) from MNIT, Jaipur in 2003. He has been working with Airports Authority of India and attached to Space Applications Centre, ISRO, Ahmedabad for the implementation of Indian SBAS–GAGAN. His research activities include ionospheric and tropospheric effects on GNSS and positioning. He received Ph.D. from M. L. Sukhadia University, Udaipur in 2013.

Sneha Yadav completed her B.Sc., and M.Sc., (Physics), and Ph.D. from the Barkatullah University, India in 2004, 2006 and 2012, respectively. During 2013–2016, she was a postdoctoral fellow at Physical Research Laboratory, India. Presently, she is working as an INSPIRE Faculty at Space Physics Laboratory, VSSC, India. Her research interest includes ionospheric modeling and space weather impact on the ionosphere.

R. Sridharan (M' 68) a Ph.D. from Gujarat University (1983), India, pioneered the development of techniques for daytime airglow measurements and for in situ probing of ionosphere/thermosphere. He specializes in Optical Aeronomy, Space-borne instruments, GPS-based research/applications pertaining to equatorial/low latitudes and also Planetary Sciences. The current focus is on developing reliable forecasting tool for ionospheric scintillations that affect satellite-based navigation.

Mala S. Bagiya received her Ph.D. degree in physics from Saurashtra University, Rajkot, India in 2010. She is working the field of upper atmospheric physics. Her research interests include dynamics of equatorial F-region ionospheric irregularities, space weather effects on the upper atmosphere and lithospheric–atmospheric coupling.

P. V. Khekale received his B.E. (Electronics and Telecom.) from Pune University in 1978. He joined Space Applications Centre (ISRO) in 1983 and has worked in the areas of digital image processing, DTH, satellite navigation, etc. He was responsible for the establishment of a network of TEC and scintillation monitoring receivers under GAGAN project.

Pan Singh received Bachelor's degree in Electronics and Communication engineering. He joined Indian Engineering Services in 1985 and then joined Airports Authority of India in 1987. He has served at various vital positions in Communication Navigation and Surveillance department. Currently, his responsibility as the General Manager includes GAGAN operations, Aviation safety, Human Resource management, etc.

S. V. Satish M.Sc. (Maths) joined Airports Authority of India in 1986 and had served at various crucial positions in Air Traffic Management. He is currently heading the department of Aviation Safety and IT as Executive Directors. He has played a key role in the implementation, certification and commissioning of GAGAN.